Ultrafast optical spectroscopy of the lowest energy excitations in the Mott insulator compound YVO_3: Evidence for Hubbard-type excitons

Fabio Novelli,[1] Daniele Fausti,[1,2,*] Julia Reul,[3] Federico Cilento,[2] Paul H. M. van Loosdrecht,[4] Agung A. Nugroho,[5] Thomas T. M. Palstra,[4] Markus Grüninger,[3] and Fulvio Parmigiani[1,2]

[1]*Department of Physics, Università degli Studi di Trieste, 34127 Trieste, Italy*

[2]*Sincrotrone Trieste SCpA, 34127 Basovizza, Italy*

[3]*Department of Physics, University of Cologne, 50923 Köln, Germany*

[4]*Zernike Institute for Advanced Materials, University of Groningen, 9747 AG Groningen, The Netherlands*

[5]*Faculty of Mathematics and Natural Sciences, Jl. Ganesa 10, Bandung 40132, Indonesia*

(Received 23 May 2012; published 31 October 2012)

Revealing the nature of charge excitations in strongly correlated electron systems is crucial to understanding their exotic properties. Here we use broadband ultrafast pump-probe spectroscopy in the visible range to study low-energy transitions across the Mott-Hubbard gap in the orbitally ordered insulator YVO_3. Separating thermal and nonthermal contributions to the optical transients, we show that the total spectral weight of the two lowest peaks is conserved, demonstrating that both excitations correspond to the same multiplet. The pump-induced transfer of spectral weight between the two peaks reveals that the low-energy one is a Hubbard exciton, i.e., a resonance or a nearly bound state between a doublon and a holon. Finally, we speculate that the pump-driven spin disorder can be used to quantify the kinetic energy gain of the excitons in a ferromagnetic environment.

DOI: 10.1103/PhysRevB.86.165135 PACS number(s): 78.47.D−, 71.27.+a, 71.35.−y, 75.25.Dk

I. INTRODUCTION

The physical properties of materials characterized by strong electron-electron interactions are determined by the competitive minimization of the potential energy and kinetic energy of the electrons. While the potential energy is lowest for localized electrons, the tendency to a metallic state increases it at the expense of the kinetic energy. The fine-tuning of the system's parameters results in the exotic ordering phenomena characterizing transition metal oxides (TMOs).[1] In a Mott-Hubbard insulator the lowest electronic excitation across the gap creates, in the most simple case, an empty site (a holon in the lower Hubbard band) and a doubly occupied site (a doublon in the upper Hubbard band).[2] In the single-band Hubbard model, the energy of this transition is solely determined by the on-site Coulomb repulsion between electrons leading to an effective energy cost U. Typically, the holon and doublon are not bound to each other, but more composite excited states have been predicted by the extended Hubbard model including nonlocal interactions.[3–7] In particular, a new kind of bound state between a holon and a doublon was recently introduced and named the Hubbard exciton (HE).[8–11] While the formation of HEs can be driven by a drop of Coulomb energy,[12,13] as in simple semiconductors, a kinetic energy loss could further stabilize the excitonic state in magnetic environments.[10,14–16] Nonlocalized HEs have been extensively studied in the framework of high-temperature superconductivity[17,18] in relation to the proposed kinetic-energy-driven formation of the condensate.[19–21]

In this report we show that an extended HE picture rationalizes the optical properties of YVO_3, a case study for Mott-insulating TMOs. In this scenario, the optical transition (see Fig. 1) observed in the reflectivity at 2.4 eV reflects the "single-particle" (SP) band, whereas the one at 1.8 eV is attributed to an excitonic resonance related to a gain in kinetic energy.[22] Our pump-probe spectroscopic measurements in the 1.65–2.75 eV range allow us to determine the temporal evolution of the spectral weight, $SW = \int_0^\infty \sigma_1(\omega)d\omega$, in the optical conductivity $\sigma_1(\omega)$ of each absorption band separately. We find that the SW is directly transferred between the two peaks, confirming the excitonic nature of the low-energy feature. Together with this, we measured both thermal and nonthermal effects and quantified the kinetic energy contribution to the formation of the HE. Our study provides a new methodology, based on both static and time-domain spectroscopy, which can be used to unravel the complex nature of high-energy excitations in insulating TMOs and, more broadly, to study kinetic energy-based mechanisms in strongly correlated materials.

The observation of multiple temperature-induced magnetization reversals[23] accompanied by a series of structural,[24] magnetic,[25] and orbital phase transitions[26] turned the Mott insulator YVO_3 into a case study among TMOs. At room temperature YVO_3 has a $Pbnm$ orthorhombic crystal structure, where each VO_6 octahedron is tilted and distorted. V^{3+} ions have a $3d^2$ electronic configuration[27] so that two electrons occupy the t_{2g} orbitals. At 200 K a phase transition to a monoclinic phase ($Pb11$[28] or $P2_1/c$[24,29,30]) occurs with G-type orbital order (G-OO). In this state, d_{yz} or d_{zx} orbitals are alternately occupied both in the ab plane and along the c axis [Fig. 2(e)]. While still monoclinic and G-OO, at $T_{SO} = 116$ K, a C-type spin order (C-SO) emerges, characterized by an antiferromagentic (AFM) spin configuration in the ab plane and a ferromagnetic (FM) order along the c axis [Fig. 2(f)]. For further cooling below $T_{Néel} = 77$ K, a structural, orbital, and magnetic transition occurs: the system recovers the $Pbnm$ crystalline structure, while the orbital ordering switches to C type (C-OO) and the spin order to G type (G-SO).[31–34] The low-temperature phase is not discussed further in the following because the crystals tend to break at the low-temperature phase transition, often leading to a loss of thermal contact[22] and strong average heating.

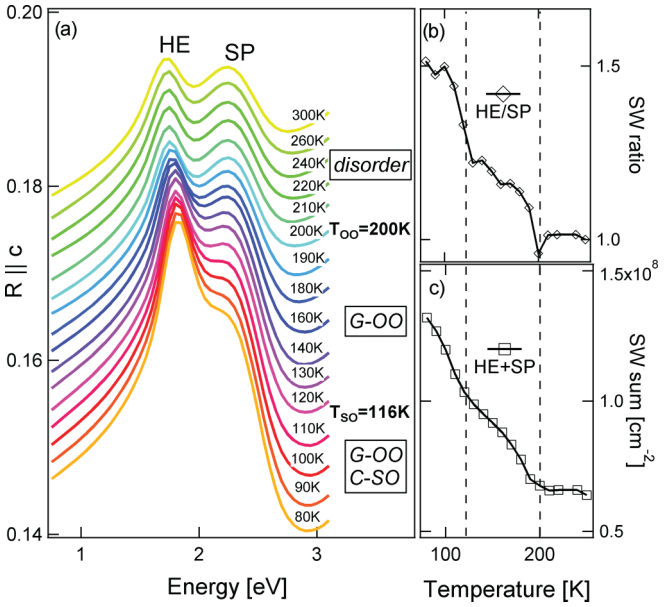

FIG. 1. (Color online) (a) Reflectivity for $E||c$ as a function of temperature of YVO_3 obtained by ellipsometry data. (b) The ratio between the spectral weight of the excitonic and single-particle bands increases rapidly while entering the G-OO phase and increases further at the spin ordering temperature. (c) Both the SP and the HE spectral weights increase upon cooling. In (b) and (c) dashed lines represent the transition temperatures towards the orbital ordering ($T_{OO} = 200$ K) and the additional spin ordering ($T_{SO} = 116$ K). In (b) the ratio is normalized to the value at 300 K. Note that the reflectivity measurements in (a) are displaced for clarity from the measurement at 80 K.

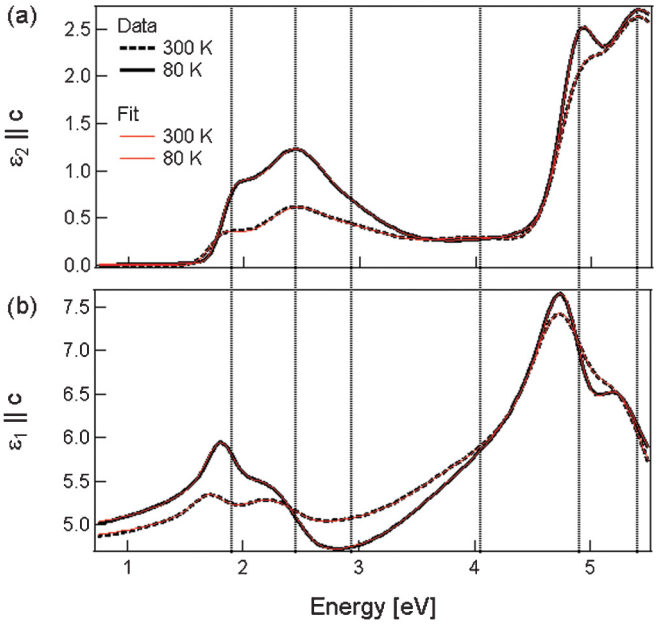

FIG. 2. (Color online) Dielectric constant of YVO_3 for $E||c$ at 80 and 300 K. (a) Imaginary and (b) real parts of the dielectric constant of YVO_3 measured by ellipsometry[22] along the c axis at 80 and 300 K. Dashed vertical lines mark the positions of the central frequencies of the oscillators used to perform the static fitting procedure (see text).

II. METHODS

Our time-domain spectroscopic technique offers a direct view on pump-induced changes in reflectivity over a broad frequency range. This has significant advantages compared to a single-color pump-probe experiment. It allows, for instance, determination of the time-dependent SW of the different features characterizing the optical response. The observation of a direct transfer of SW between the HE and the SP band in YVO_3 is the central experimental result of this study. We start our analysis from a model for the static data. We fitted ϵ_2 by a sum of six Gaussian peaks and a Tauc-Lorentz oscillator for the transition at lower energy (HE), ϵ_1 by the Kramers-Kronig consistent functional form. With these line shapes, which have been justified and extensively used to address amorphous and locally disordered materials,[35,36] we obtain static fits of very good quality (Fig. 3). The dielectric expressions used are

$$\epsilon_2(\omega) = L_a(\omega) + L_b(\omega) + \ldots + L_g(\omega),$$

where $L_a(\omega) = \frac{1}{\omega}\frac{a\omega_a\gamma_a(\omega-\text{gap})^2}{(\omega^2-\omega_a^2)^2+\omega^2\gamma_a^2}$ if $\omega >$ gap and $L_a(\omega) = 0$ elsewhere. L_c, L_d, L_e, L_f, and L_g are analogous to $L_b(\omega) = b(e^{-4\ln 2\frac{(\omega-\omega_b)^2}{\gamma_b^2}} - e^{-4\ln 2\frac{(\omega+\omega_b)^2}{\gamma_b^2}})$; a, b, and c are the amplitudes, and ω_i and γ_i the central frequencies and widths for $i = a,b,c\ldots$,

$$\epsilon_1(\omega) = 1 + D_a(\omega) + D_b(\omega) + \cdots + D_g(\omega),$$

where $D_a(\omega)$ has the Jellison form[37,38] and the other terms $[D_b(\omega), \ldots, D_g(\omega)]$ are proper sums of Dawson's functions.[39] By simultaneous fitting of both the real and the imaginary part of the dielectric constant, we were able to obtain a series of continuously varying parameters. In the c-axis fitting the Gaussian centered at 33 000 cm^{-1} ($\approx$4 eV) loses SW below 140 K: we left this oscillator free to vary, as attempts to block it produce a much worse fit. For the same reason we bind the central frequency of another oscillator at 23 000 cm^{-1} ($\approx$2.9 eV). These assumptions are justified by the overall good fits of the static optical properties. It should be noted that these approximations, which have been made to give a good description of the static optical properties outside of the interest range for the time-domain data, do not affect the outcome of the time-domain fits. This was verified by performing time-domain fits with different sets of parameters. The SWs were computed as $\int_0^{23\,000}\omega\epsilon_2(\omega)d\omega$, with ω in cm^{-1} and $\epsilon_2(\omega)$ composed only of the HE peak or the SP peak.[40]

In order to calculate the pump-induced evolution of the SW of the two bands from the transient reflectivity data, we proceed as follows. We consider the model used to fit the static ellipsometry data, we calculate the equilibrium reflectivity (R_0), and we fit the measured transient reflectance $[\Delta R_{\text{exp}}(t)/R_{\text{exp}}]$ with a differential model $[(R(t) - R_0)/R_0]$, where $R(t)$ is a model for the perturbed reflectivity obtained by variation of the parameters used to fit the equilibrium data as a function of the pump-probe delay t. The values of the oscillator parameters obtained by this fitting procedure at different times are used to calculate the evolution of the SW:

$$\Delta\text{SW}(t) = \text{SW}^{\text{pumped}}(t) - \text{SW}^{\text{static}}(T),$$

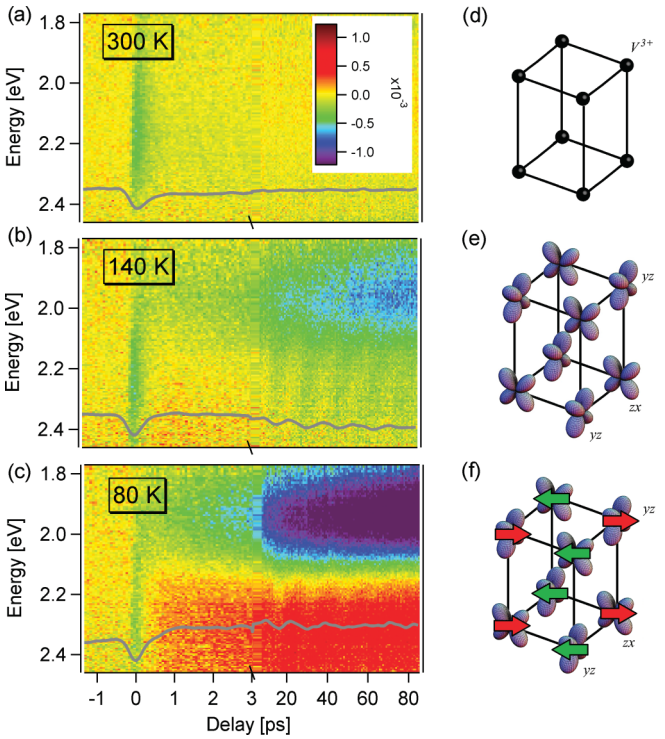

FIG. 3. (Color online) Broadband transient reflectivity spectra. Transient reflectivity as a function of energy and pump-probe delay for the three phases: (a) disordered, $T = 300$ K; (b) G-type orbital order, $T = 140$ K; and (c) C-type spin order, $T = 80$ K. Gray lines represent the transient reflectivity at the fixed energy of 2.33 eV as retrieved in standard single-color pump-probe measurements. The oscillatory trend was assigned to acoustic vibrations[48] and is ignored. For (a), (b), and (c), the respective ordering patterns are sketched in (d), (e), and (f).

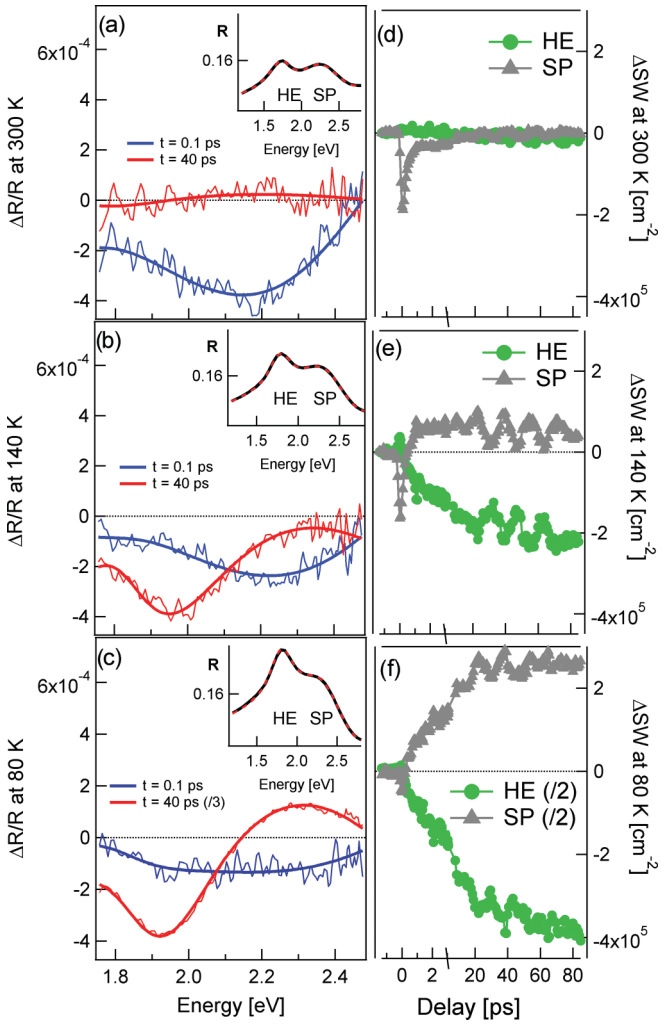

FIG. 4. (Color online) From transient reflectivity to spectral weight. The transient reflectance was fitted using a variational approach on the static fit. (a, b, c) Transient reflectance for two characteristic times, typical of the "fast" and "slow" dynamics, at 300, 140, and 80 K, respectively, and the relative variational fit. Insets: Static reflectance for the different phases.[22] (d, e, f) Time evolution of the SW variations in the different phases (see text).

where $\mathrm{SW}^{\mathrm{pumped}}(t)$ is calculated from the fitting parameters of $R(t)$, and $\mathrm{SW}^{\mathrm{static}}(T)$ is obtained from the static reflectivity at temperature T (both SWs are calculated by the numerical intergration described earlier).

III. RESULTS

All phase transitions can be identified by monitoring the optical properties of YVO_3. The region of the optical spectra that is particularly sensitive to the orbital physics is the visible range, just above the gap of about 1.6 eV. The two peaks characterizing the reflectivity, with energies of 1.8 eV (HE) and 2.4 eV (SP) are largely debated[22,28,32,34,41–46] and commonly assigned to $d_i^2 d_j^2$-$d_i^1 d_j^3$ transitions between two different V_i and V_j sites.[28,41] However, the assignment to different multiplets of the peaks observed in the optical data has been controversial.[22,28,32,41] For $E||c$ both excitations, at 1.8 and 2.4 eV, gain SW with decreasing temperature and approaching the spin-ordering transition at $T_{\mathrm{SO}} = 116$ K [Fig. 1(c)], indicating that they both correspond to the same high-spin multiplet.[22] The SW gain with decreasing temperature is much stronger for the lower peak, which has tentatively been attributed to excitonic behavior. In this scenario, the lower peak is an excitonic resonance, i.e., a nearly bound state within the continuum. This is supported by a comparison of optical data with band-structure calculations and photoemission data.[22] In fact from Hund's rules we expect the kinetic energy contribution to the formation of the Hubbard exciton to be more relevant for parallel alignment of spins such as along c in the C-SO phase.[10]

In order to distinguish the effects of temperature and spin or orbital disorder we performed pump-probe reflectivity measurements. The complex dielectric function $\varepsilon(\omega)$ was measured by ellipsometry; for details see Ref. 22. The static normal-incidence reflectivity $R(\omega)$ reported in Fig. 1 was calculated from $\varepsilon(\omega)$. Broadband supercontinuum probe experiments combined with an ultrafast optical pump at 1.6 eV were performed on freshly polished ac-oriented YVO_3 samples mounted on the cold finger of a helium-flow cryostat. The reflectivity changes as a function of the pump-probe delay $\frac{\Delta R}{R}(\omega,t) = \frac{R(\omega,t)-R(\omega)}{R(\omega)}$ induced by 80-fs pump pulses ($E_{\mathrm{pump}} = 1.6$ eV, fluence < 4 mJ/cm^2, at a 40-KHz repetition

rate, with polarization parallel to the a axis) were measured as a function of the energy (for 1.65 eV $< E_{\text{probe}} <$ 2.75 eV) and temperature. The linearity of the response was checked in all phases up to 8 mJ/cm^2.

The three phases are characterized by the different responses summarized in Fig. 2 for probe polarization parallel to the c axis (see Supplemental Material[47]). At room temperature, the pump-probe measurements are solely characterized by a very fast negative variation of the reflectivity (decay time $\tau \approx 0.5$ ps) extending over the investigated spectral region [Fig. 2(a)]. On the contrary, the low-temperature phases are characterized by a more composite optical response with fast and slow components, confirming previously reported single-color measurements.[48,49] The time-domain reflectivity measurements in the G-OO phase (116 K $< T <$ 200 K) are characterized by a slow negative response centered at 1.94 eV [Fig. 2(b)], which becomes more pronounced as the temperature is lowered [Fig. 2(c)]. Finally, entering the C-SO phase (80 K $< T <$ 116 K) a positive variation of the reflectivity appears at energies higher than 2.1 eV.

IV. DISCUSSION

Among the 21 parameters used to fit the features in the static $\varepsilon(\omega)$, the minimal set of parameters needed to obtain good differential fits at all temperatures and times contains only the following four: the amplitude, central frequency, and width of the oscillator describing the HE band and the amplitude of the SP band. Figures 4(a)–4(c) show typical fits obtained for the fast (blue curves) and slow response (red curves) in the different phases. The obtained values for the temporal evolution of the oscillator parameters are used to calculate the time-domain evolution of the SW. The variation of the SW for the two bands in time is calculated independently as the difference of the SW calculated for the model at a specific time [$\text{SW}^{\text{pumped}}_{\text{HE,SP}}(t)$] minus the static SW ($\text{SW}^{\text{static}}_{\text{HE,SP}}$) (each SW is calculated by numerical integration of the optical conductivity describing the band).

The time dependence of $\Delta\text{SW}(t)$ of the HE and SP bands as a function of the pump-probe delay t is reported in Figs. 4(d)–4(f) for three significant temperatures. The fast response ($t < 3$ ps) in all phases is entirely described by a variation of the SP peak, while the HE peak seems to be unaffected by photoexcitation in the first few picoseconds. This evidence can be rationalized as ground-state depletion, confirming that only the higher energy optical transition is of SP origin. In fact, if the SP band is related to a delocalized excitation and the HE band has "more" of a localized origin, one would expect only the SP band to be perturbed "immediately" by pump excitation. On the other hand, the slow response ($t > 10$ ps) revealed in the orbitally ordered phases is related to SW changes in both the HE and the SP bands. The time-domain response cannot be accounted for by photoinduced heating. The SW of both oscillators increases upon cooling (Fig. 1) and it is therefore expected that transient laser-induced heating would result in a decrease in the SW of both the SP and the HE bands. However, the time-domain measurements (Fig. 2) reveal that only the SW of the HE peak decreases, while the SP band shows the opposite behavior, which rules out a simple heating effect. The nonthermal SW gain of the high-energy oscillator (Fig. 5) lasts

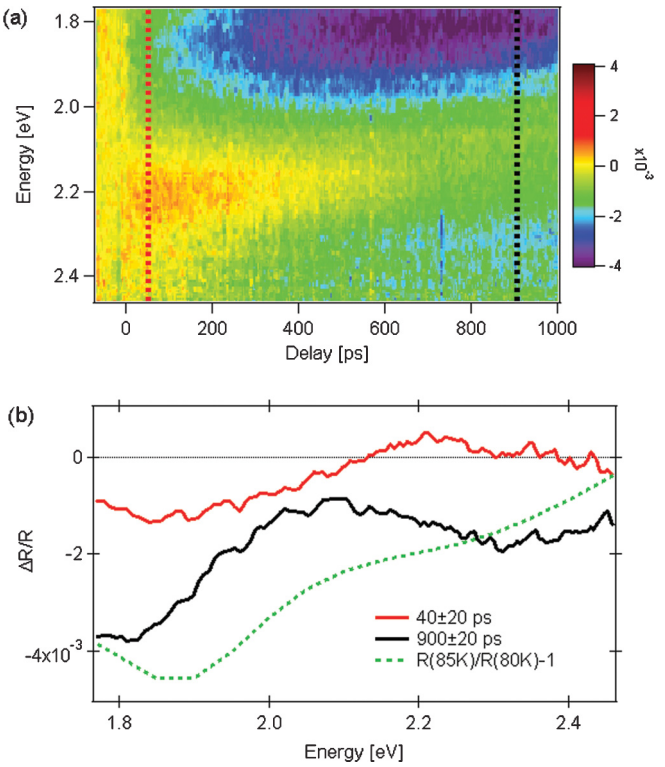

FIG. 5. (Color online) Long-time-scale pump-probe measurement at 80 K. (a) Time-domain reflectivity data at 80 K. Note that the fast response visible in Fig. 2 is absent because of the coarse temporal step used. (b) Transient reflectance at $t = 40$ ps (red curve) and 900 ps (black curve). The expected thermal response, $[R^{\text{static}}(85\text{ K}) - R^{\text{static}}(80\text{ K})]/R^{\text{static}}(80\text{ K})$, is shown for comparison [dotted (green) curve].

up to ≈400 ps, and only at longer times do the measurements indicate a SW loss for both oscillators. A comparison between the green and the black curves in Fig. 5(b) reveals that 1 ns after photoexcitation the degrees of freedom have not reached thermal equilibrium.

Following those considerations we analyze the transient SW measured at $t > 20$ ps (well beyond the electronic relaxation) as resulting from a thermal contribution and a nonthermal one. The thermal contribution to the SW variation in the HE and SP peaks [$\text{SW}^{\text{static}}_{\text{HE}}(T + \Delta T)$ and $\text{SW}^{\text{static}}_{\text{SP}}(T + \Delta T)$] can be calculated by interpolation of the temperature behavior of the static measurements at $T + \Delta T$, where ΔT is the photoinduced heating obtained from thermodynamic considerations (see Supplemental Material[47]). The SW variations of nonthermal origin can therefore be calculated by subtracting the thermal contribution to the experimental values:

$$\Delta\text{SW}^{\text{nonthermal}}_{\text{HE}} = \text{SW}^{\text{pumped}}_{\text{HE}}(50\text{ ps}) - \text{SW}^{\text{static}}_{\text{HE}}(T + \Delta T)$$

and

$$\Delta\text{SW}^{\text{nonthermal}}_{\text{SP}} = \text{SW}^{\text{pumped}}_{\text{SP}}(50\text{ ps}) - \text{SW}^{\text{static}}_{\text{SP}}(T + \Delta T)$$

for the HE and SP bands, respectively, where $\text{SW}^{\text{pumped}}_{i}(50\text{ ps})$ (i = HE, SP) are the means of the measured photoexcited SWs at $t = 50 \pm 30$ ps after pump arrival.

The nonthermal components of the pump-driven SW variations at different equilibrium temperatures are reported in

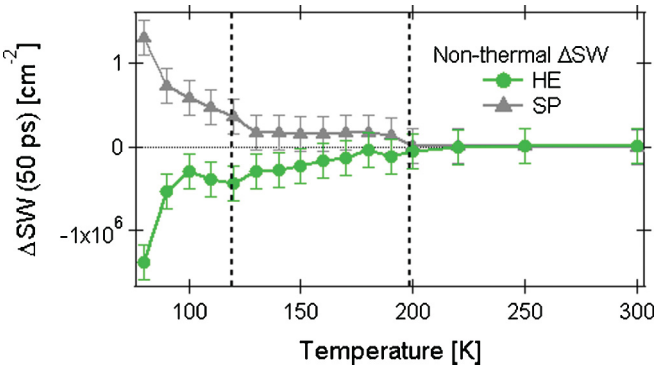

FIG. 6. (Color online) Nonthermal spectral weight (SW) changes of the HE and SP peaks. The excitonic nature of the low-energy transition is revealed by the direct SW exchange between the two excitations (see text). The error bars were estimated from the fitting procedure.

Fig. 6. It is evident that the nonthermal contributions consist of a direct exchange of SW between the HE and the SP peaks: this result proves that the two lowest lying optical excitations belong to the same multiplet and that the 1.8 eV transition is of an excitonic nature.[22] Moreover, the increase in the photoinduced SW transfer from the HE to the SP peak in the C-SO phase (Fig. 6, at $T < 116$ K) highlights the kinetic energy contribution to the formation of the HE peak.

We argue that the SW loss of the HE peak in favor of the SP peak is driven by pump-induced spin disorder (Fig. 7). Two adjacent and c-oriented orbital chains of YVO_3 in the G-OO/C-SO phase are sketched in the first row in Fig. 7. The spin order is FM along the c axis ($J_c < 0$), while it is AFM in the orthogonal direction ($J_a > 0$). Photoexctitation (a axis polarized) transfers charges between chains, leaving one excess electron at a site and one vacancy at the nearest-neighbor site as depicted in Fig. 7 ($t = 0$). Magnetic coupling between an excited and a nonexcited site along c changes as a consequence of this charge redistribution (J_c^*). This dramatic perturbation of the spin coupling can be grasped by the following considerations. The Goodenough-Kanamori rules,[50] stating that the superexchange coupling J between half-filled and empty orbitals is negative, are consistent with the FM order observed along the c axis. At the simplest, the pump-driven changes in the orbital occupation lead to a switch from FM to AFM exchange coupling. The electronic subsystem relaxes within a few picoseconds (t_1), while the spins remain locally perturbed (tilted blue arrows in Fig. 7, for $t = t_1$). We argue that, the orbital angular momentum being completely quenched, the coupling mechanism allowing the magnetic subsystem to transfer energy to other degrees of freedom is very weak. Therefore, the local perturbation of the spins diffuses (t_2), leading to spin disorder. This partially suppresses the kinetic energy gain of the HE peak and leads, subsequently, to a nonthermal SW transfer to the SP peak. A fully thermalized state is achieved only on much longer time scales (>1 ns) through spin-lattice coupling.[49]

In conclusion, here we have revealed the nature of the two lowest energy peaks detected in the 1- to 3-eV optical spectra

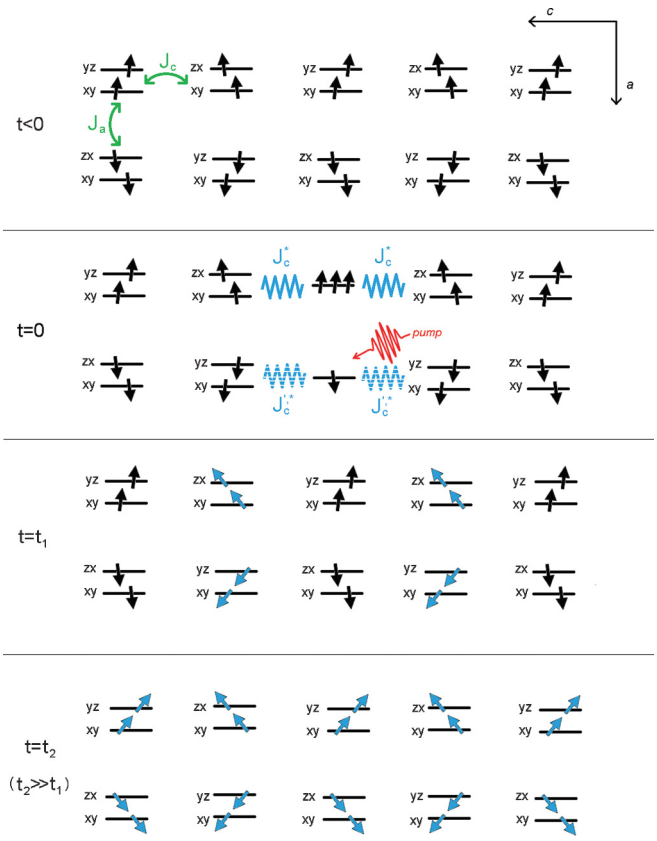

FIG. 7. (Color online) Nonthermal spin disorder. YVO_3 is in the G-OO/C-SO phase; t indicates the pump-probe delay ($t < 0$ represents the unperturbed state). The photoexcited holons and doublons perturb the magnetic coupling locally along the FM chain J_c^* ($J_c^{'*}$) ($t = 0$, central site). The photoexcited electrons relax within a few picoseconds ($t \approx t_1$), leaving a local perturbation on the spin system. The spin disorder diffuses along the FM chains on a longer time scale ($t = t_2$), resulting in SW transfer between the HE and the SP peaks (see text).

of the orbitally ordered Mott insulator YVO_3. This finding was made possible by out-of-equilibrium experiments. The results show how time-domain broadband optical spectroscopies can disentangle the thermal and nonthermal contributions to the optical transients of properly excited states across a Mott-Hubbard gap. In particular, we have proven that the total SW is conserved during the de-excitation process, hence revealing that the low-energy feature is a Hubbard exciton, i.e., a resonance or a nearly bound state between a doublon and a holon. This observation, otherwise not conceivable using spectroscopies in the frequency domain, suggests that the optically pump-driven spin disorder can be used to quantify the kinetic energy gain of the excitons in the FM phase.

ACKNOWLEDGMENTS

The authors are grateful to M. Malvestuto, J. van den Brink, L. Hozoi, and K. Wohlfeld for useful discussion. We acknowledge G. R. Blake for reviewing the manuscript.

*Correspondence author: daniele.fausti@elettra.trieste.it

[1] M. Imada, A. Fujimori, and Y. Tokura, Rev. Mod. Phys **70**, 1039 (1998).

[2] A. Fujimori and Y. Tokura, *Spectroscopy of Mott Insulators and Correlated Metals* (Springer-Verlag, Berlin, 1994).

[3] J. van den Brink, M. B. J. Meinders, J. Lorenzana, R. Eder, and G. A. Sawatzky, Phys. Rev. Lett. **75**, 25 (1995).

[4] R. Neudert, M. Knupfer, M. S. Golden, J. Fink, W. Stephan, K. Penc, N. Motoyama, H. Eisaki, and S. Uchida, Phys. Rev. Lett. **81**, 657 (1998).

[5] A. Hubsch, J. Richter, C. Waidacher, K. W. Becker, and W. von der Linden, Phys. Rev. B **63**, 205103 (2001).

[6] S. Wall *et al.*, Nat. Phys. **7**, 114 (2011).

[7] R. G. Leigh and P. Phillips, Phys. Rev. B **79**, 245120 (2009).

[8] F. H. L. Essler, F. Gebhard, and E. Jeckelmann, Phys. Rev. B **64**, 125119 (2001).

[9] H. Matsueda, T. Tohyama, and S. Maekawa, Phys. Rev. B **71**, 153106 (2005).

[10] A. Gössling, R. Schmitz, H. Roth, M. W. Haverkort, T. Lorenz, J. A. Mydosh, E. Müller-Hartmann, and M. Grüninger, Phys. Rev. B **78**, 075122 (2008).

[11] Y. Matiks, P. Horsch, R. K. Kremer, B. Keimer, and A. V. Boris, Phys. Rev. Lett. **103**, 187401 (2009).

[12] F. B. Gallagher and S. Mazumdar, Phys. Rev. B **56**, 15025 (1997).

[13] E. Jeckelmann, Phys. Rev. B **67**, 075106 (2003).

[14] F. C. Zhang and K. K. Ng, Phys. Rev. B **58**, 13520 (1998).

[15] D. G. Clarke, Phys. Rev. B **48**, 7520 (1993).

[16] P. Wrobel and R. Eder, Phys. Rev. B **66**, 035111 (2002).

[17] Y. Y. Wang, F. C. Zhang, V. P. Dravid, K. K. Ng, M. V. Klein, S. E. Schnatterly, and L. L. Miller, Phys. Rev. Lett. **77**, 1809 (1996).

[18] E. Collart, A. Shukla, J. P. Rueff, P. Leininger, H. Ishii, I. Jarrige, Y. Q. Cai, S. W. Cheong, and G. Dhalenne, Phys. Rev. Lett. **96**, 157004 (2006).

[19] J. E. Hirsch, Science **295**, 2226 (2002).

[20] H. J. A. Molegraaf, C. Presura, D. van der Marel, P. H. Kes, and M. Li, Science **295**, 2239 (2002).

[21] P. Phillips, Rev. Mod. Phys. **82**, 1719 (2010).

[22] J. Reul, A. A. Nugroho, T. T. M. Palstra, and M. Grüninger, Phys. Rev. B **86**, 125128 (2012).

[23] Y. Ren *et al.*, Nature **396**, 441 (1998).

[24] G. R. Blake, T. T. M. Palstra, Y. Ren, A. A. Nugroho, and A. A. Menovsky, Phys. Rev. B **65**, 174112 (2002).

[25] C. Ulrich, G. Khaliullin, J. Sirker, M. Reehuis, M. Ohl, S. Miyasaka, Y. Tokura, and B. Keimer, Phys. Rev. Lett. **91**, 257202 (2003).

[26] M. Noguchi, A. Nakazawa, S. Oka, T. Arima, Y. Wakabayashi, H. Nakao, and Y. Murakami, Phys. Rev. B **62**, R9271 (2000).

[27] H. F. Pen, M. Abbate, A. Fuijmori, Y. Tokura, H. Eisaki, S. Uchida, and G. A. Sawatzky, Phys. Rev. B **59**, 7422 (1999).

[28] A. A. Tsvetkov, F. P. Mena, P. H. M. van Loosdrecht, D. van der Marel, Y. Ren, A. A. Nugroho, A. A. Menovsky, I. S. Elfimov, and G. A. Sawatzky, Phys. Rev. B **69**, 075110 (2004).

[29] M. Reehuis, C. Ulrich, P. Pattison, B. Ouladdiaf, M. C. Rheinstädter, M. Ohl, L. P. Regnault, M. Miyasaka, Y. Tokura, and B. Keimer, Phys. Rev. B **73**, 094440 (2006).

[30] T. A. W. Beale, R. D. Johnson, Y. Joly, S. R. Bland, P. D. Hatton, L. Bouchenoire, C. Mazzoli, D. Prabhakaran, and A. T. Boothroyd, Phys. Rev. B **82**, 024105 (2010).

[31] H. Sawada, N. Hamada, K. Terakura, and T. Asada, Phys. Rev. B **53**, 12742 (1996).

[32] Z. Fang, N. Nagaosa, and K. Terakura, Phys. Rev. B **67**, 035101 (2003).

[33] Z. Fang and N. Nagaosa, Phys. Rev. Lett. **93**, 176404 (2004).

[34] M. De Raychaudhury, E. Pavarini, and O. K. Andersen, Phys. Rev. Lett. **99**, 126402 (2007).

[35] S. K. O'Leary and P. K. Lim, Solid State Commun. **104**, 17 (1997).

[36] S. A. MacDonald, C. R. Schardt, D. J. Masiello, and J. H. Simmons, J. Non-Cryst. Solids **275**, 72 (2000).

[37] G. E. Jellison and F. A. Modine, Appl. Phys. Lett. **69**, 371 (1996).

[38] G. E. Jellison and F. A. Modine, Appl. Phys. Lett. **69**, 2137 (1996).

[39] D. De Sousa, M. Malki, and P. Echegut, J. Non-Cryst. Solids **352**, 769 (2006).

[40] It should be noted that the spectral weights reported in Ref. 22 are computed from Lorentzian line shapes, giving rise to slightly different absolute values.

[41] S. Miyasaka, Y. Okimoto, and Y. Tokura, J. Phys. Soc. Jpn. **71**, 2086 (2002).

[42] R. J. O. Mossanek and M. Abbate, Phys. Rev. B **76**, 035101 (2007).

[43] R. J. O. Mossanek, M. Abbate, P. T. Fonseca, A. Fujimori, H. Eisaki, S. Uchida, and Y. Tokura, Phys. Rev. B **80**, 195107 (2009).

[44] Y. Otsuka and M. Imada, J. Phys. Soc. Jpn. **75**, 124707 (2006).

[45] G. Khaliullin, P. Horsch, and A. M. Oles, Phys. Rev. B **70**, 195103 (2004).

[46] A. M. Oles, G. Khaliullin, P. Horsch, and L. F. Feiner, Phys. Rev. B **72**, 214431 (2005).

[47] See Supplemental Material at http://link.aps.org/supplemental/10.1103/PhysRevB.86.165135 for intermediate temperatures and details on the thermodynamic model.

[48] D. A. Mazurenko, A. A. Nugroho, T. T. M. Palstra, and P. H. M. van Loosdrecht, Phys. Rev. Lett. **101**, 245702 (2008).

[49] R. V. Yusupov, D. Mihailovic, C. V. Colin, G. R. Blake, and T. T. M. Palstra, Phys. Rev. B **81**, 075103 (2010).

[50] H. Weihe and U. Güdel, Inorg. Chem. **36**, 3632 (1997).